**Electronic Supplementary Material (ESI) for New Journal of Chemistry**

# Synthesis and X-ray crystallographic analysis of free base and hexafluorophosphate salts of 3,4-dihydroisoquinolines from the Bischler-Napieralski reaction

Carlos E. Puerto Galvis,[a,b] Cristian C. Granados,[c] Vladimir V. Kouznetsov[a]* and Mario A. Macías*[c]

[a.] *Laboratorio de Química Orgánica y Biomolecular, CMN, Universidad Industrial de Santander. Parque Tecnológico Guatiguará, Km 2 Vía Refugio, Piedecuesta 681011, Colombia. E-mail: kouznet@uis.edu.co, vkuznechnik@gmail.com; Tel: +57 7 634 4000 Ext. 3593.*

[b.] *Laboratorio de Química Orgánica Aplicada, Universidad Manuela Beltrán, Cl. 33 # 26-34, Bucaramanga, Colombia, PBox, 680002. Fax/Tel: +57 7 6525202.*

[c.] *Crystallography and Chemistry of Materials, CrisQuimMat, Department of Chemistry. Universidad de los Andes. Carrera 1 No. 18A 10, Bogotá 111711, Colombia. *E-mail: ma.maciasl@uniandes.edu.co*

**List of contents**

## 1. General procedure and characterization data of compounds 2a-b and 2d

A 10 mL reactor vial equipped with a magnetic stir bar was charged with the corresponding *N*-phenylethyl cinnamamide **1a-d** (2 mmol) and 1-butyl-3-methylimidazolium hexafluorophosphate ([bmim]$PF_6$) or acetonitrile (1 mL). The resulting solution was stirred at room temperature until complete dissolution of the amide and phosphoryl chloride ($POCl_3$) (3 mmol, 1.5 equiv.) was added in one portion. Then, the system was heated at 50 °C for 24 hours. After cooling to room temperature, crushed ice was slowly added to the reaction mixture until complete precipitation of the respective hexafluorophosphate salt **2a-b**. The solid was filtered, washed with distilled water and dried under vacuum. For 3,4-dihydroisoquinoline **2d** the after the reaction was completed, the solvent was evaporated under reduced pressure and the crude reaction mixture was suspended in crushed ice, treated with aqueous $NaHCO_3$ (1 M) to pH = 8, and then extracted with $CH_2Cl_2$ (3 x 10 mL). Finally, the combined organic extracts were dried over $Na_2SO_4$, concentrated, and purified by flash column chromatography on silica gel (10% MeOH in $CH_2Cl_2$).

**6-Methoxy-1-styryl-3,4-dihydroisoquinolin hexafluorophosfate (2a):** Following general procedure, compound **2a** was obtained as an orange solid (0.52 g, 61 %); $R_f$ [$CH_2Cl_2$/MeOH 2:1] = 0.35; mp 197-199 °C (from EtOH/AcOEt 5:2 ratio); IR (KBr Disk) $\nu_{max}/cm^{-1}$: 2977 (OCH3), 2838 (NH+), 1619 (C=N), 1558 (C-N), 1280 (C-O), 848 (P-F); NMR $\delta^1$H(400 MHz, $CDCl_3$, $Me_4Si$), *J* values are given in Hz: 10.05 (1H, br s, N*H*$^+$), 7.95 (1H, d, *J* = 16.1, C*H*Ph), 7.91 (1H, d, *J* = 8.8, 8-$H_{Ar}$), 7.73 (2H, dd, *J* = 7.9, 1.3, 5' and 9'-$H_{Ar}$), 7.54-7.44 (3H, m, 6', 7' and 8'-$H_{Ar}$), 7.27 (1H, d, *J* = 16.2, C*H*), 7.02 (1H, dd, *J* = 8.9, 2.5, 7-$H_{Ar}$), 6.94 (1H, d, *J* = 2.6, 5-$H_{Ar}$), 3.98 (3H, s, OC$H_3$), 4.01-3.96 (2H, m, -C$H_2$N), 3.16-3.11 (2H, m, -C$H_2$Ph); NMR $\delta^{13}$C(101 MHz, $CDCl_3$, $Me_4Si$): 167.2, 150.7 (+), 142.0, 136.6, 133.7 (+), 133.6, 132.8 (+), 129.7 (2C, +), 129.6 (2C, +), 117.9, 115.4 (+), 114.9 (+), 114.5 (+), 58.6 (-), 56.3 (+), 26.7 (-) (For **2a**, drops of EtOH were added to improve solubility); HRMS (ESI): calcd. for $C_{18}H_{18}NO$ [M-$PF_6$]: 264.1383, found: 264.1391.

**6,7-Dimethoxy-1-(3,4,5-trimethoxystyryl)-3,4-dihydroisoquinolin hexafluorophosfate (2b):** Following general procedure, compound **2b** was obtained as an orange solid (0.91 g, 86 %); $R_f$ [$CH_2Cl_2$/MeOH 2:1] = 0.20; mp 191-193 °C (from EtOH/AcOEt 5:2 ratio); IR (KBr Disk) $\nu_{max}/cm^{-1}$: 2946 ($OCH_3$), 2838 (NH+), 1604 (C=N), 1465 (C-N), 1280 (C-O), 833 (P-F); NMR δ $^1$H(400 MHz, $CDCl_3$, $Me_4Si$), *J* values are given in Hz: 9.92 (1H, br s, N*H*$^+$), 7.86 (1H, d, *J* = 16.3, C*H*Ph), 7.30 (1H, s, 8-$H_{Ar}$), 7.16 (1H, d, *J* = 16.0, C*H*), 7.00 (2H, s, 5' and 9'-$H_{Ar}$), 6.90 (1H, s, 5-$H_{Ar}$), 4.05 (3H, s, OC$H_3$), 3.96 (3H, s, OC$H_3$), 3.95 (3H, s, OC$H_3$), 3.93 (6H, s, OC$H_3$), 3.92-3.90 (2H, m, C$H_2$N), 3.08 (2H, t, *J* = 7.6, C$H_2$Ph); NMR $\delta^{13}$C(101 MHz, $CDCl_3$,

$ME_4Si$): 168.7, 161.8, 154.0 (+), 151.1 (2C), 149.3 (2C), 140.0, 135.0, 128.9, 115.0 (+), 114.5 (+), 113.5 (+), 107.7 (+, 2C), 56.8 (+, 2C), 56.7 (+, 2C), 56.7 (+), 41.2 (-), 26.3 (-); HRMS (ESI): calcd. for $C_{22}H_{26}NO_5$ [M-$PF_6$]: 384.1805, found: 384.1808.

**6,7-Dimethoxy-1-(4-methoxyphenethyl)-3,4-dihydroisoquinoline (2d):** Following general procedure, compound **2d** was obtained as a yellow solid (0.37 g, 78 %); $R_f$ [$CH_2Cl_2$/MeOH 8:1] = 0.51; mp 143-145 °C (from EtOH); IR (KBr Disk) $\nu_{max}/cm^{-1}$: 2915 ($CH_2$-Ar), 2854 ($OCH_3$), 1650 (C=N), 1511 (C-N), 1465 ($CH_2$-Ar), 1280 (C-C) ; NMR $\delta^1$H(400 MHz, $CDCl_3$, $Me_4Si$), *J* values are given in Hz: 7.15 (2H, d, *J* = 8.6, 6' and 8'-$H_{Ar}$), 6.95 (1H, s, 8-$H_{Ar}$), 6.84 (2H, d, *J* = 8.7, 5' and 9'-$H_{Ar}$), 6.70 (1H, s, 5-$H_{Ar}$), 3.91 (3H, s, OC$H_3$), 3.86 (3H, s, OC$H_3$), 3.78 (3H, s, OC$H_3$), 3.67-3.61 (2H, m, -C$H_2$N), 2.97-2.92 (4H, m, 2' and 3'-C$H_2$), 2.66-2.57 (2H, m, -C$H_2$Ph). NMR $\delta^{13}$C(101 MHz, $CDCl_3$, $Me_4Si$): 166.0, 157.9, 150.7, 147.5, 134.1, 131.5, 129.4 (2C, +), 122.0, 113.9 (2C, +), 110.3 (+), 108.5 (+), 56.2 (+), 56.0 (+), 55.3 (+), 47.0 (-), 38.2 (-), 32.4 (-), 25.9 (-). HRMS (ESI): calcd. for $C_{20}H_{24}NO_3$ $[M+H]^+$: 326,1751, found: 326,1747.

## 2. Hirshfeld Surface analysis of 1-phenethyl-3,4-dihydroisoquinoline 2d and 6-methoxy-1-styryl-3,4-dihydroisoquinolin-hexafluorophosfate 2a

With the aim of complementing the information regarding the packing in crystals of **2d** and **2a** we performed Hirshfeld surface analysis using *CrystalExplorer*.[1] The obtained Hirshfeld surfaces mapped over $d_{norm}$ for **2d** and **2a**, Fig. 1(*a*) and (b), exhibited the characteristic red spots over the surfaces indicating close contact points of interest.

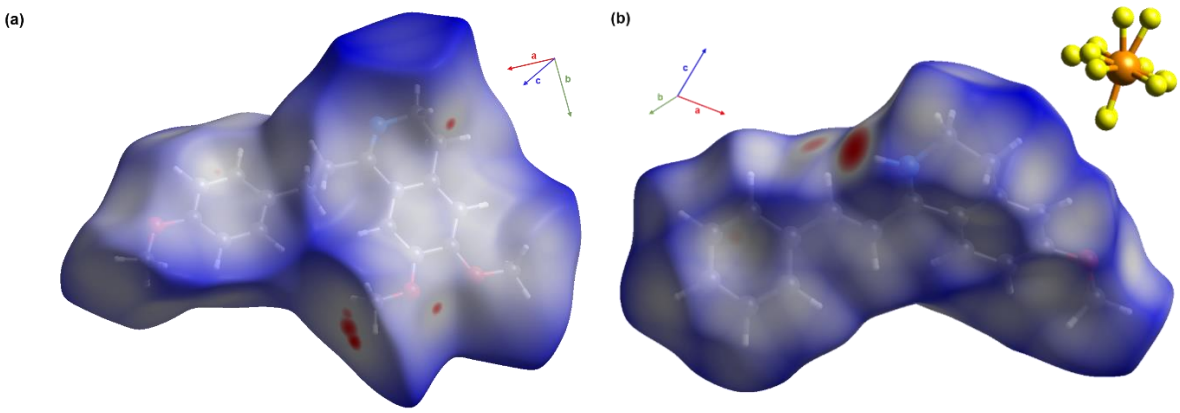


**Figure 1.** Hirshfeld surfaces mapped over $d_{norm}$ for (*a*) **2d** over the ranges -0.0818 to +2.9204 and (*b*) **2a** over the ranges -0.4349 to +1,2104 arbitrary units.

The surface for **2d** presented 6 contact points of interest, labeled from 1 – 6 in Fig. 2(*a*) and (*b*), that were represented by 3 pairs of different types of close contacts: 2 H···H, 2 C—H···O, and 2 C—H···π. Additionally, the intensity of the red spots is related to the strength of the intermolecular contact, which, in turn, is reflected directly in the distance of the contacts.[2] In this case, as seen in Fig. 2(*a*) and (*b*), the contact points with the highest intensity on the surface were the ones associated with the H···H interactions between the central molecule, *i.e.* the one enveloped by the Hirshfeld surface, and the neighboring molecules colored in red. This implies that the non-covalent H···H close contacts are the ones with the smallest distance and, perhaps, contribute to most of the interactions present in the structure, while C—H···π contacts have the largest distance (Table 1) and lowest contribution.

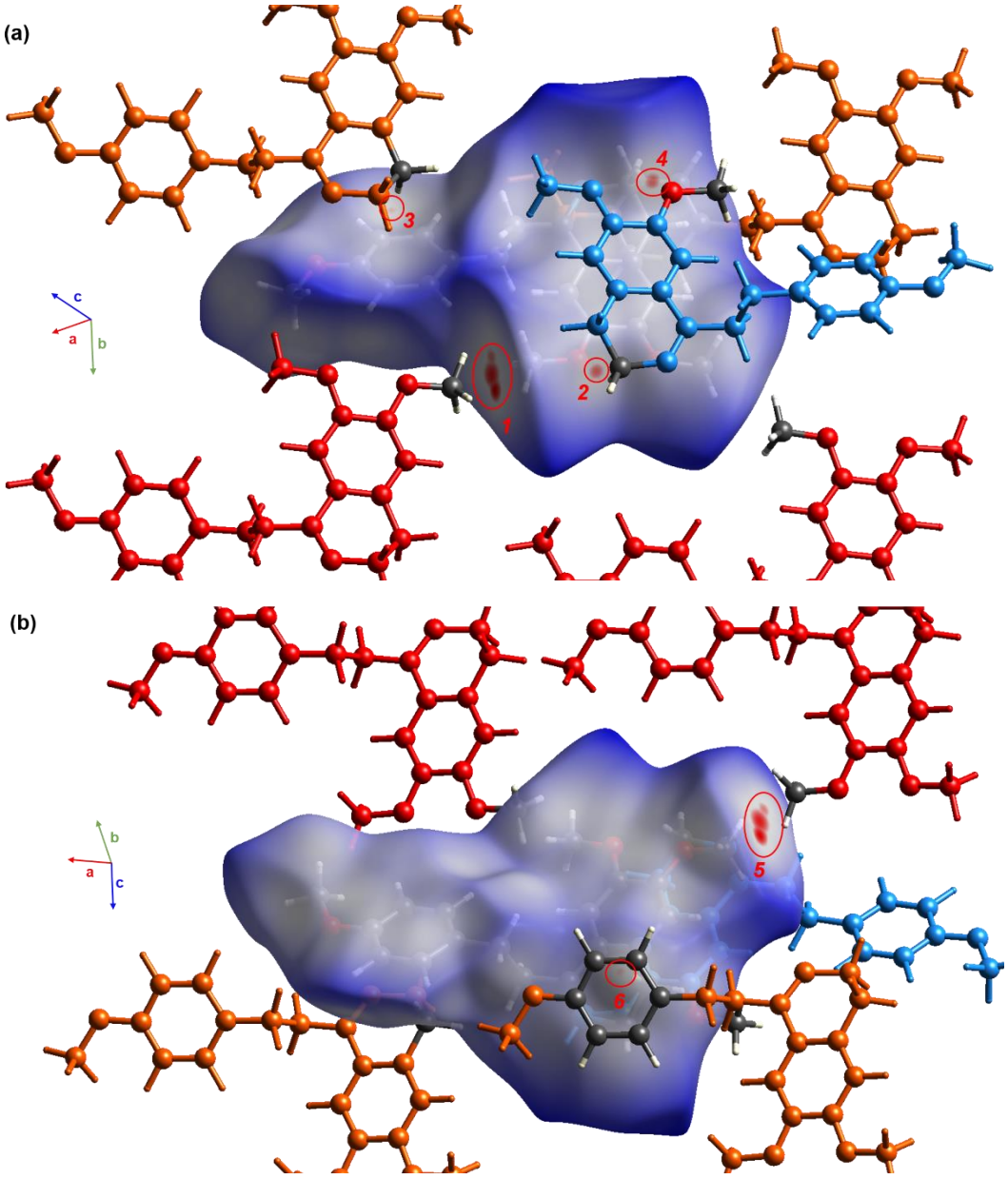


**Figure 2.** Two views of the Hirshfeld surface for **2d** mapped over $d_{norm}$ showing (*a*) 4 close contacts and (*b*) 2 close contacts labeled in red. The color of the neighboring molecules to the surface represents a type of close contact: red, H···H contacts; blue, C—H···O contacts; orange, C—H···π. The uncolored fragments or atoms in a molecule are the ones involved directly in the contacts.

This observation becomes clearer, from a quantitative point of view, by observing the contribution of each contact to the total fingerprint plot area for **2d** in Fig. 3(*a*)-(*d*). From this figure, it is straightforward that the H···H close contacts account for most of the total area, followed by the C—H···O and the C—H···π contacts in lower proportion. Considering this, it is reasonable to think that most of the packing in the crystal of **2d** is governed by dispersion interactions. Another reason to support this idea is the spread of points attributed to H···H contacts over $d_i = d_e \approx 2.4$ Å, which implies that the dispersion interaction is distributed not

only over short but also long distances in the crystal. Moreover, the spread of contacts over long distances indicates that the structure has a low packing density.[3]

However, there are several features about the fingerprint plot that reveal in more detail the packaging and the interactions of the crystal. For example, one of them is the display of 'wings' at the upper left and bottom right of the plot which are distinctive of aromatic systems and have been recognized as an indicator for C—H···π interactions.[3] Additionally, other characteristic features of aromatic systems that can be observed on the plot are the 'herringbone' motif, *i.e.* the spikes near $d_i = d_e \approx 1.1$ Å, and the bright blue-green area centered at $d_i = d_e \approx 1.8$ Å. which is an indicator of π ···π stacking interactions,[3] in this case, involving. This can be seen in the expanded crystal structure (Fig. 1) where the 3,4-dihydroisoquinoline motifs stack along the $[\bar{1}01]$ direction.

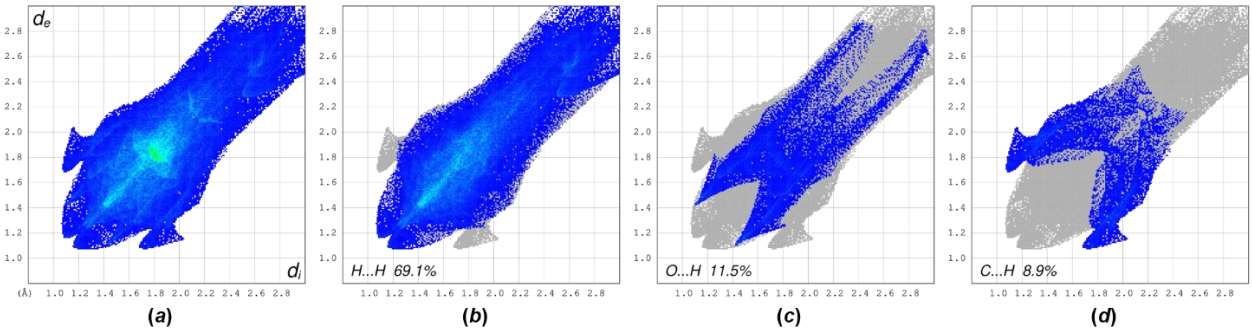


**Figure 3.** (*a*) Full fingerprint plot for **2d** and decomposition of the plot into (*b*) H···H, (*c*) O···H and (*d*) C···H contacts contribution to the total area.

On the other hand, by mapping other properties over the Hirshfeld surface, such as shape-index, more information about the crystal packing nature can be observed. From Fig. 3(*a*) and (*b*), points 3 and 6 were assigned to C—H···π contacts over the surface. However, this assignment can also be addressed by looking at the Hirshfeld surface for **2d** mapped over the shape-index property (Fig. 4). As seen in earlier work, when using the shape-index property in aromatic systems, the appearance of bright red spots surrounded by small blue regions indicate the presence of C—H···π as well as π ···π stacking interactions.[2]

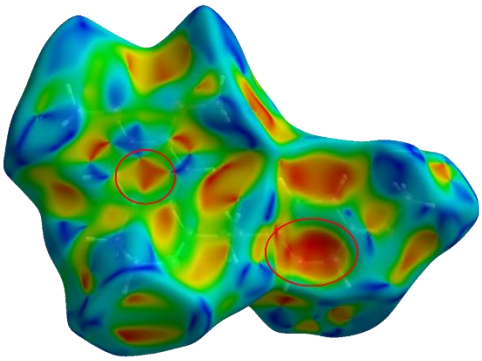

**Figure 4.** Hirshfeld surface for **2c´** mapped over the shape-index property showing the characteristic regions for π ···π interactions.

Furthermore, the Hirshfeld surface for **2a** mapped over $d_{norm}$ exhibited 6 close contacts of interest as well. Although the number of close contacts for both structures is the same, the contribution of the involved interactions differs as shown in Fig. 5(*a*) and (*b*). One difference between **2d** and **2a** is that there are no C—H···O or H···H interactions in **2a**. Instead, these interactions are replaced for 4 X—H···F (X = N, C) contacts in which X is nitrogen in one of them. Also, these X—H···F have the highest intensity on the surface meaning they represent the shortest distances (Table 2) and have the highest contribution to the interactions present in the structure.

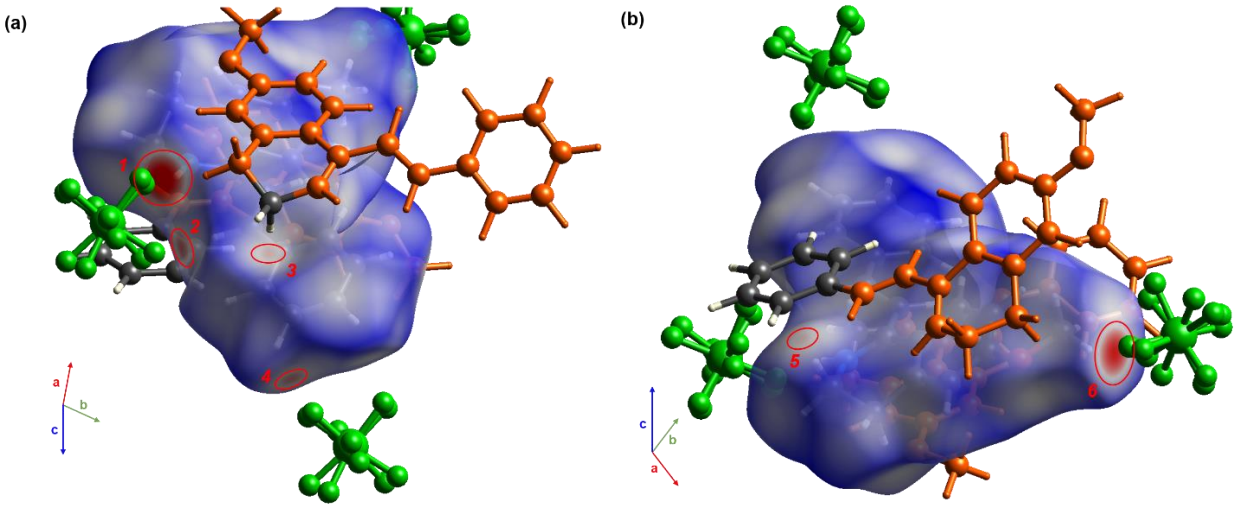


**Figure 5.** Two views of the Hirshfeld surface for **2a** mapped over $d_{norm}$ showing (*a*) 4 close contacts and (*b*) 2 close contacts labeled in red. The color of the neighboring molecules to the surface represents a type of close contact: orange, C—H···π contacts; green, X—H···F contacts (X = N, C). The uncolored fragments or atoms in a molecule are the ones involved directly in the contacts.

These differences between **2d** and **2a** are not only evident on the Hirshfeld surface; they are substantial on the fingerprint plots. In the first place, the fingerprint plots for **2a**, shown in Fig. 6(*a*)-(*d*), confirm that the X—H···F contacts account for most of the total area followed by the H···H and the C—H···π. This reveals that the packing in the crystal of **2a** is not

determined mostly by dispersion interactions, as in **2d**, but a combination with high contribution of electrostatic interactions. Additionally, these plots show that both compounds share the display of 'wings' and the bright blue-green region centered at $d_i = d_e \approx$ 1.8 Å, showing their aromatic nature and the presence of π ···π stacking interactions in their structure. Nevertheless, besides these similarities, a loss of symmetry is noticeable for the fingerprint plot of **2a**. Instead of having two spikes at the lower left and the lower right of the plot, there is only one spike. Particularly, these spikes at short distances ($d_i \approx$ 0.9/1.1 and $d_e \approx$ 1.1/0.9 Å) represent a hydrogen bond in which each spike represents a donor and an acceptor of this interaction [3]. However, the structure of **2a** only has the hydrogen bond donor in the N—H···F interaction, which represents the smallest contact distance and explains the only spike seen in Fig. 6(*a*). Apart from this feature, another visible difference is the spread of contacts at long distances. The total plot for **2a**, shows that there are no contacts over $d_e \approx$ 2.4 Å and a few over distances of $d_i \approx$ 2.4 Å which is related to a higher packing density compared with **2d**. These differences are reflected in their calculated densities, 1.027 and 1.497 g/cm$^3$ for **2d** and **2a**, respectively.

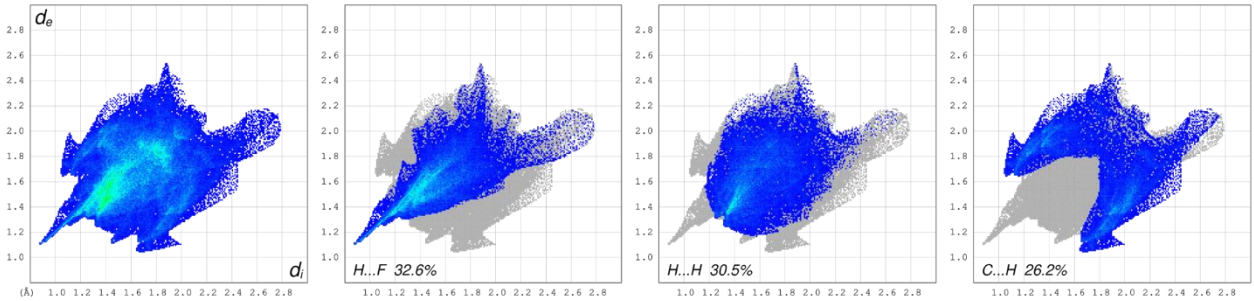


**Figure 6.** (*a*) Full fingerprint plot for **2a** and decomposition of the plot into (*b*) H···F contacts contribution, (*c*) H···H contacts contribution and (*d*) C···H contacts contribution to the total area.

**Table 1.** Distance for each type of close contact in **2c´** obtained from *Crystal Explorer 17*.

| Contact number | Type | Distance (Å) |
|---|---|---|
| 1 | H···H | 2.369 |
| 5 | H···H | 2.401 |
| 2 | C—H···O | 2.537 |
| 4 | C—H···O | 2.541 |
| 3 | C—H···π | 2.794 |
| 6 | C—H···π | 2.773 |

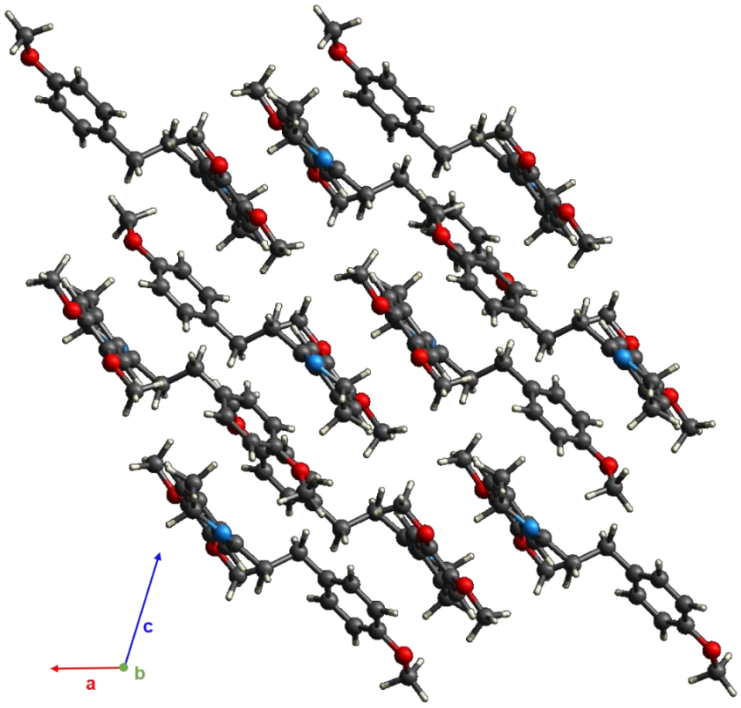


**Figure 7.** Expanded crystal structure of 1 showing the stacking along the $[\bar{1}01]$ direction.

**Table 2.** Distance for each type of close contact in **2a** obtained from *Crystal Explorer 17*.

| Contact number | Type | Distance (Å) |
|---|---|---|
| 1 | N—H···F | 1.996 |
| 2 | C—H···F | 2.338 |
| 4 | C—H···F | 2.403 |
| 6 | C—H···F | 2.069 |
| 3 | C—H···π | 2.733 |
| 5 | C—H···π | 2.731 |

## 3. Copies of $^{1}$H NMR, $^{13}$C NMR and DEPT-135 charts of 3,4-dihydroisoquinolines 2a-b and 2d.

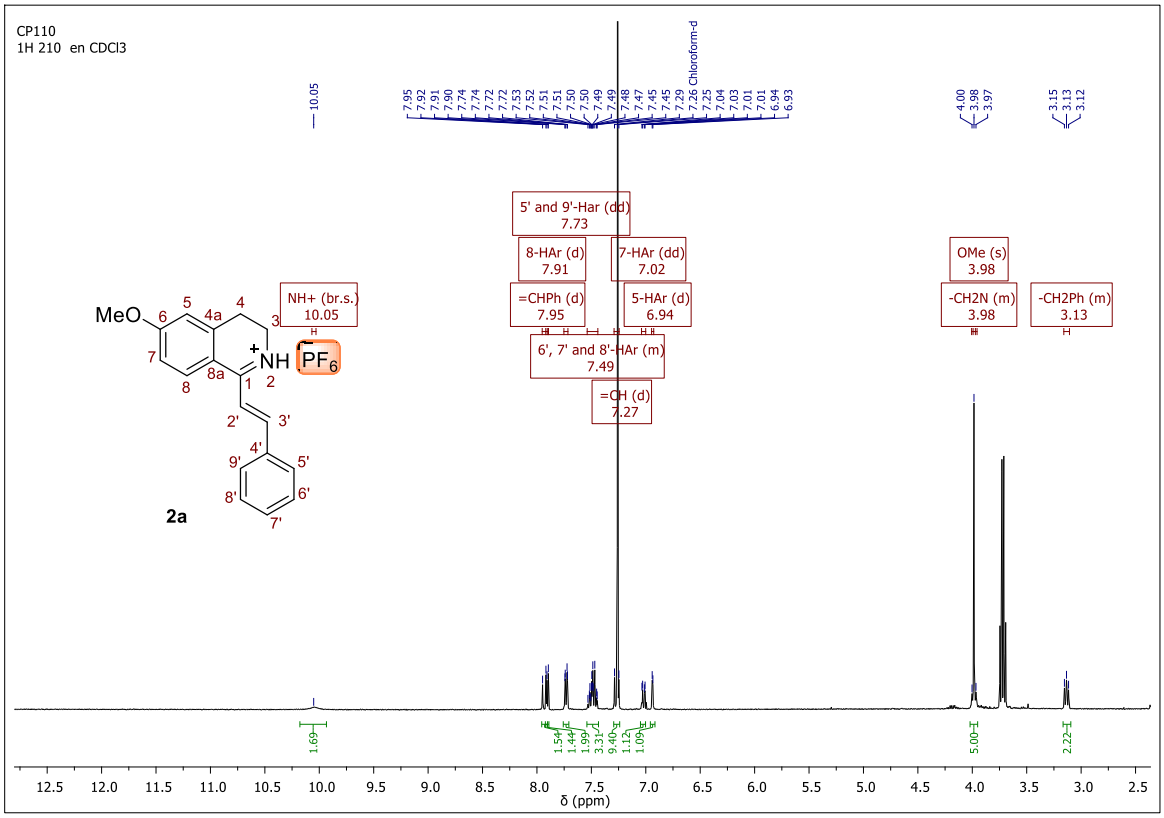


**Figure 8.** $^{1}$H-NMR spectrum of 6-methoxy-1-styryl-3,4-dihydroisoquinolin-hexafluorophosfate (**2a**)

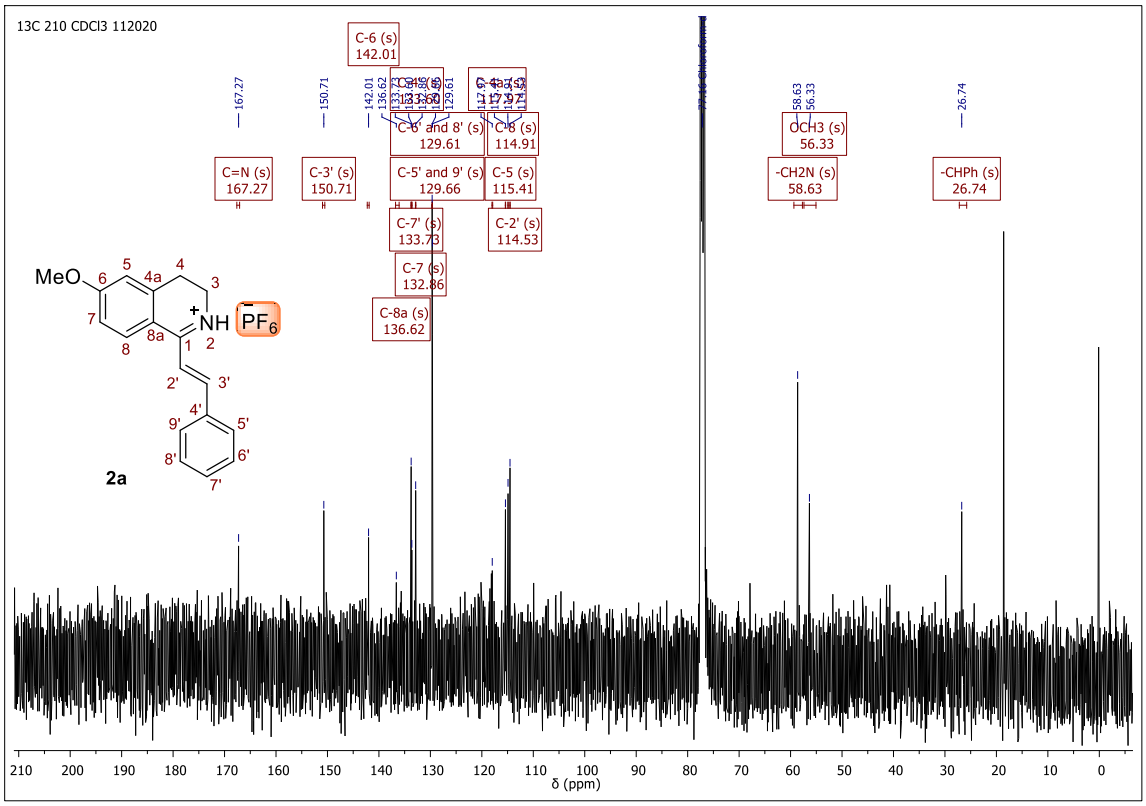


**Figure 9.** $^{13}$C-NMR spectrum of 6-methoxy-1-styryl-3,4-dihydroisoquinolin-hexafluorophosfate (**2a**)

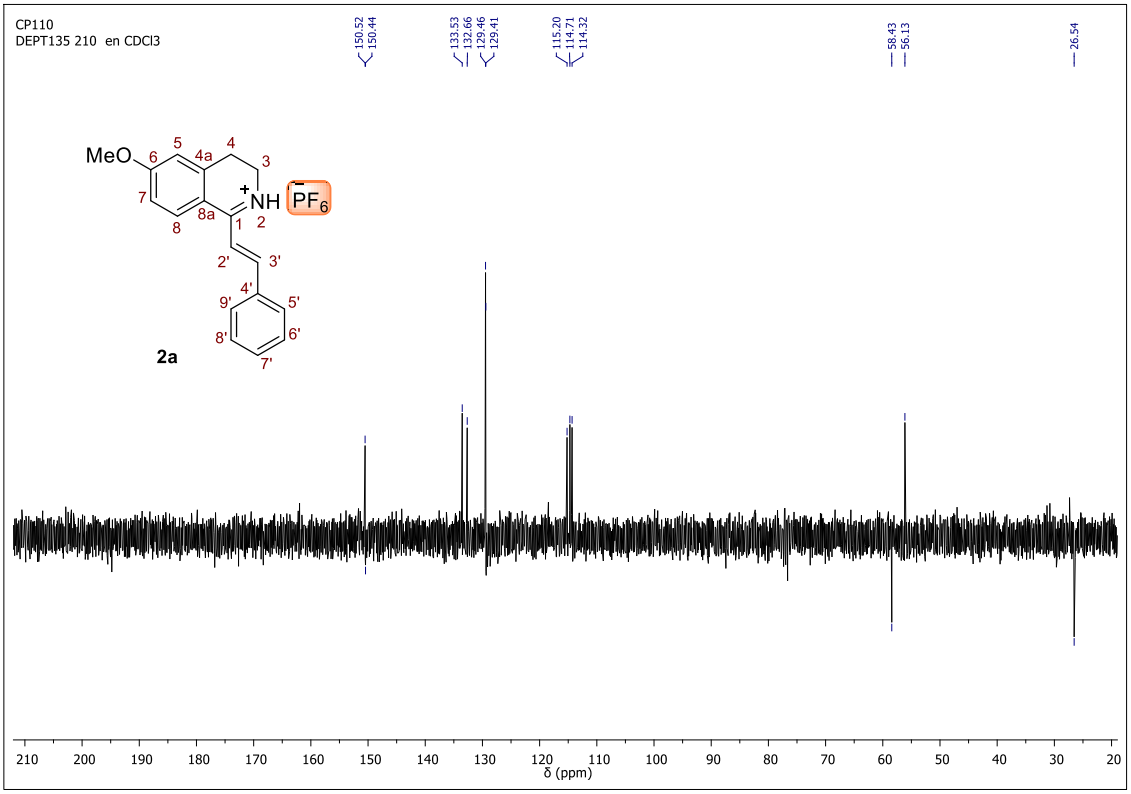


**Figure 10.** DEPT-135 spectrum of 6-methoxy-1-styryl-3,4-dihydroisoquinolin-hexafluorophosfate (**2a**)

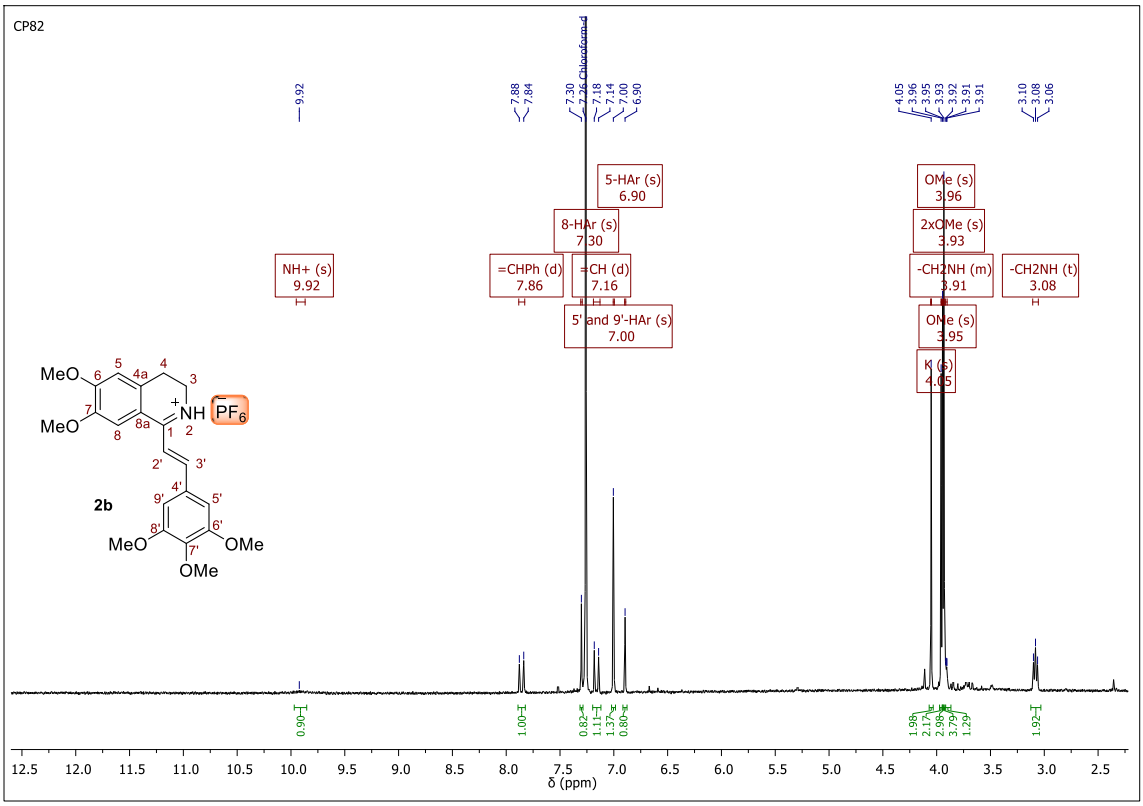


**Figure 11.** $^{1}$H-NMR spectrum of 6,7-dimethoxy-1-(3,4,5-trimethoxystyryl)-3,4-dihydroisoquinolin-hexafluorophosfate (**2b**)

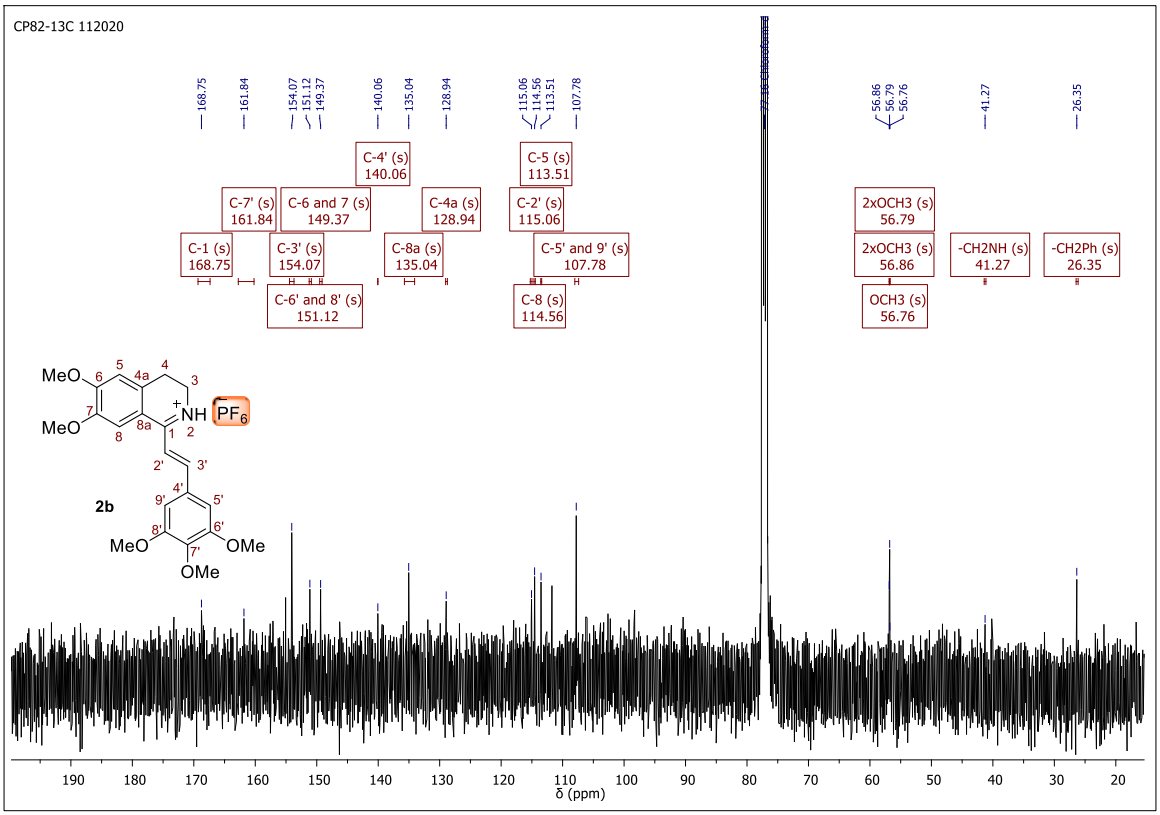


**Figure 12.** $^{13}$C-NMR spectrum of 6,7-dimethoxy-1-(3,4,5-trimethoxystyryl)-3,4-dihydroisoquinolin-hexafluorophosfate (**2b**)

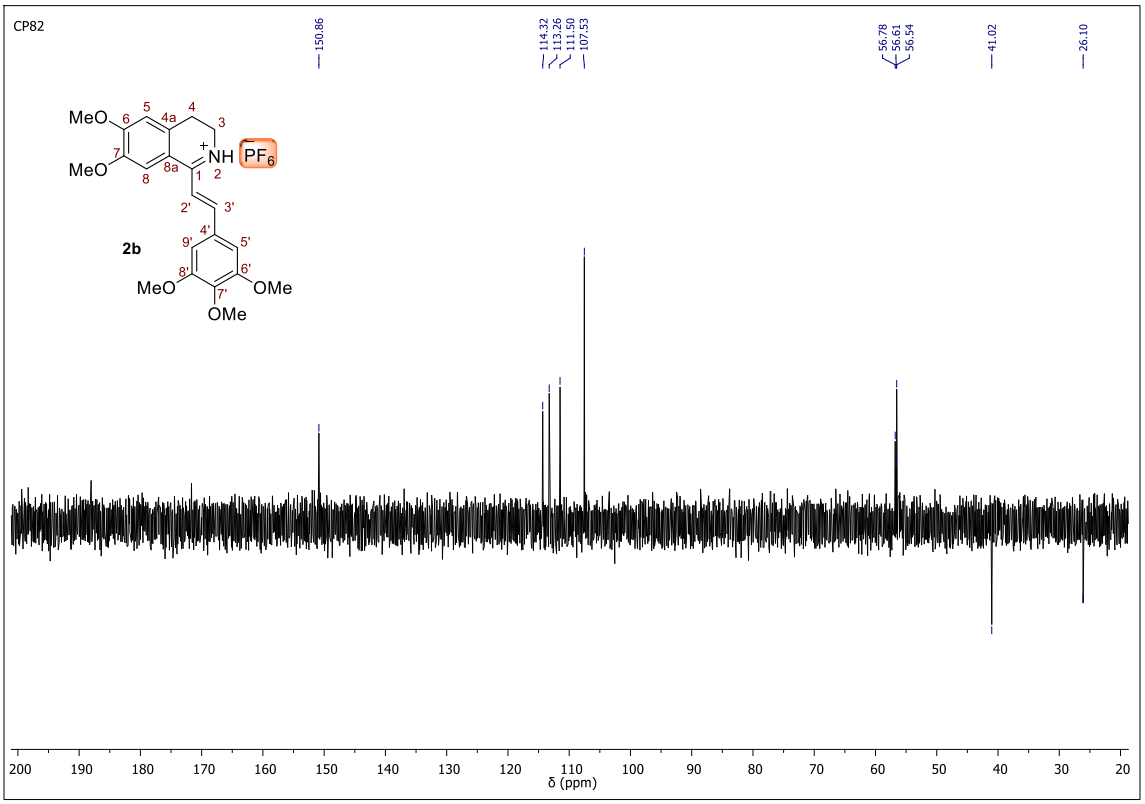


**Figure 13.** DEPT-135 spectrum of 6,7-dimethoxy-1-(3,4,5-trimethoxystyryl)-3,4-dihydroisoquinolin-hexafluorophosfate (**2b**)

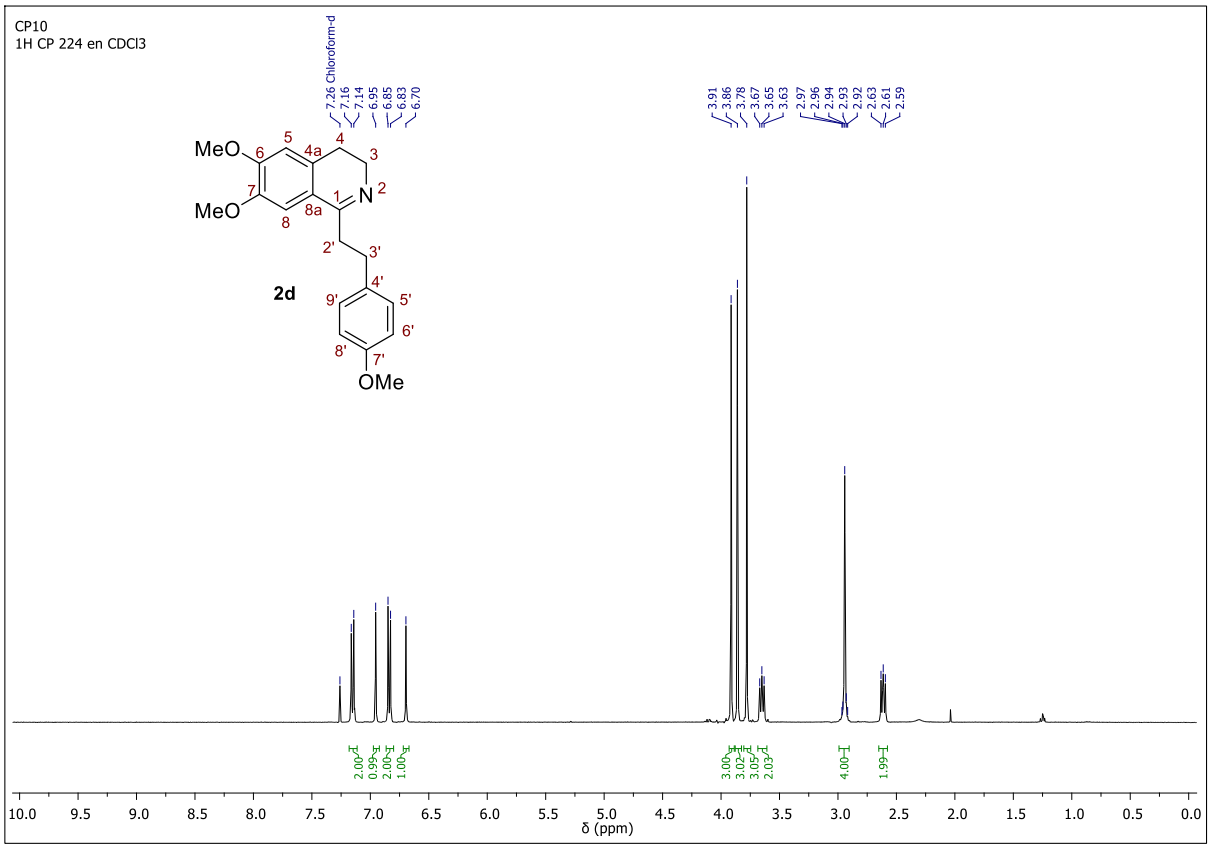


**Figure 14.** $^{1}$H-NMR spectrum of 6,7-dimethoxy-1-(4-methoxyphenethyl)-3,4-dihydroisoquinoline (**2d**).

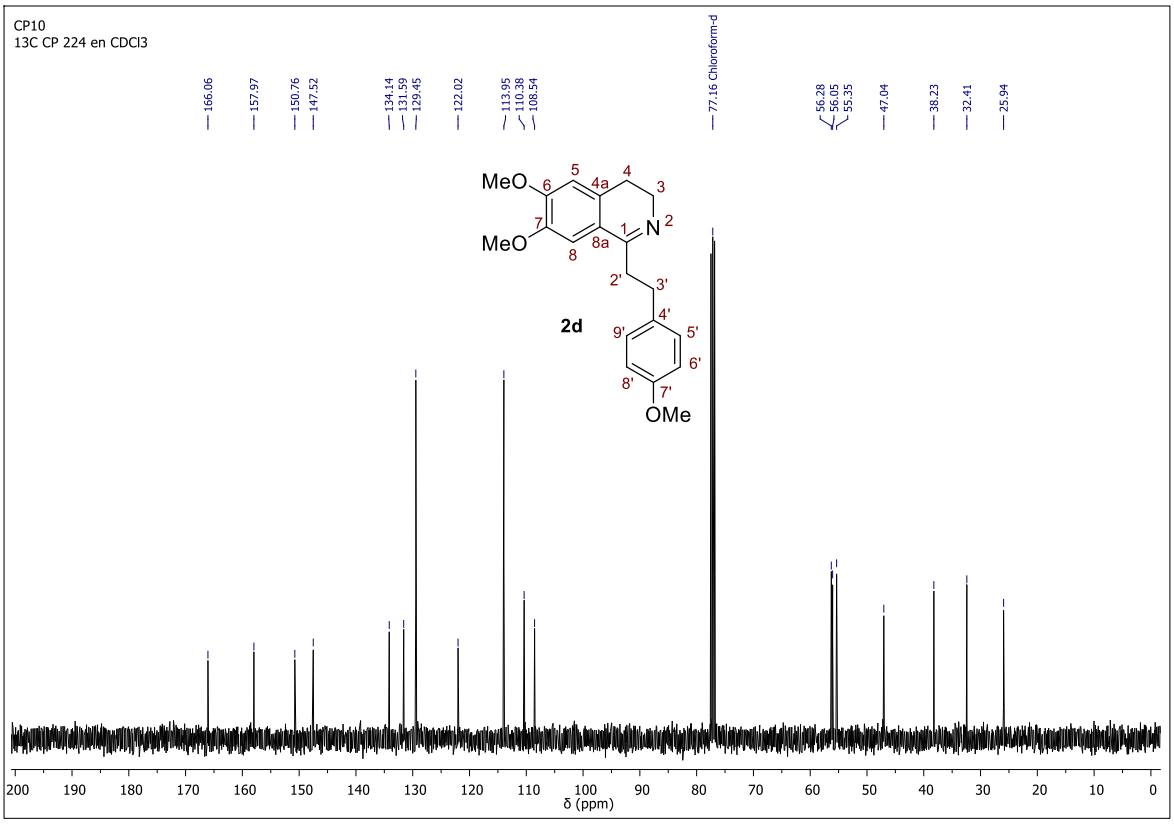


**Figure 15.** $^{13}$C-NMR spectrum of 6,7-dimethoxy-1-(4-methoxyphenethyl)-3,4-dihydroisoquinoline (**2d**).

## 4. References


1. M. J. Turner, J. J. McKinnon, S. K. Wolff, D. J. Greenwood, P. R. Spackman, D. Jayatilaka, M. A. Spackman, Crystal Explorer 17, (2017). https://crystalexplorer.scb.uwa.edu.au/ (accessed August 15, 2020).
2. S.L. Tan, M. M. Jotani, E. R. T. Tiekink, Utilizing Hirshfeld surface calculations, non-covalent interaction (NCI) plots and the calculation of interaction energies in the analysis of molecular packing, *Acta Crystallogr. Sect. E Crystallogr. Commun*. 2019, **75**, 308.
3. M. A. Spackman, J. J. McKinnon, Fingerprinting intermolecular interactions in molecular crystals, *CrystEngComm*, 2002, **4**, 378.